E-cadherin junction formation involves an active kinetic nucleation process

Kabir H. Biswas[a,1], Kevin L. Hartman[a,b,1], Cheng-han Yu[a,2], Oliver J. Harrison[c,d,e], Hang Song[c,d,e], Adam W. Smith[f,3], William Y. C. Huang[b], Wan-Chen Lin[f], Zhenhuan Guo[a], Anup Padmanabhan[a], Sergey M. Troyanovsky[g], Michael L. Dustin[h], Lawrence Shapiro[c,e], Barry Honig[c,d,e,4], Ronen Zaidel-Bar[a,i,4], and Jay T. Groves[a,b,f,j,4]

[a]Mechanobiology Institute, National University of Singapore, Singapore 117411; [b]Department of Chemistry, University of California, Berkeley, CA 94720; [c]Department of Biochemistry and Molecular Biophysics, Columbia University, New York, NY 10032; [d]Howard Hughes Medical Institute, Columbia University, New York, NY 10032; [e]Center for Computational Biology and Bioinformatics, Columbia University, New York, NY 10032; [f]Howard Hughes Medical Institute, University of California, Berkeley, CA 94720; [g]Department of Dermatology, Feinberg School of Medicine, Northwestern University, Chicago, IL 60611; [h]Kennedy Institute, Nuffield Department of Orthopaedics, Rheumatology and Musculoskeletal Sciences, University of Oxford, Headington OX3 7FY, United Kingdom; [i]Department of Biomedical Engineering, National University of Singapore, Singapore 117411; and [j]Physical Biosciences and Materials Sciences Divisions, Lawrence Berkeley National Laboratory, University of California, Berkeley, CA 94720

Contributed by Barry Honig, July 16, 2015 (sent for review May 13, 2015; reviewed by Kheya Sengupta and Sanjeevi Sivasankar)

Epithelial (E)-cadherin-mediated cell–cell junctions play important roles in the development and maintenance of tissue structure in multicellular organisms. E-cadherin adhesion is thus a key element of the cellular microenvironment that provides both mechanical and biochemical signaling inputs. Here, we report in vitro reconstitution of junction-like structures between native E-cadherin in living cells and the extracellular domain of E-cadherin (E-cad-ECD) in a supported membrane. Junction formation in this hybrid live cell-supported membrane configuration requires both active processes within the living cell and a supported membrane with low E-cad-ECD mobility. The hybrid junctions recruit α-catenin and exhibit remodeled cortical actin. Observations suggest that the initial stages of junction formation in this hybrid system depend on the *trans* but not the *cis* interactions between E-cadherin molecules, and proceed via a nucleation process in which protrusion and retraction of filopodia play a key role.

cadherin | diffusion | adhesion | nucleation | bilayer

There is a growing realization that the cellular microenvironment, including its biochemical composition as well as its geometrical and mechanical characteristics, plays a crucial role in defining the behavior of living cells. For example, growing cells on 2D surfaces patterned with extracellular matrix (ECM) (1), in 3D random ECM networks (2), or confined to microfabricated chambers (3) all reveal that geometry alone can exert specific control over cell fate. Experiments on polymer substrates with controlled rigidity demonstrate that mechanical stiffness of the microenvironment influences key cellular decisions including healthy stem cell differentiation (4) and tumorigenesis in cancer (5). Physical restriction of the clustering or transport of cell surface receptors can alter the transduction of downstream signals (6–8). The ability to control such aspects of the cellular microenvironment in a synthetic setting is key to the advancement of in vitro live cell technologies.

Epithelial (E)-cadherin-mediated adhesion is a prominent feature of epithelial sheets throughout vertebrates and related receptors are similarly used in invertebrates. E-cadherin, a type I cadherin adhesion receptor, is the main component of epithelial adherens junctions and is important for the development and remodeling of epithelial tissues in all Metazoans (9–11). Mutations in the E-cadherin gene can result in the loss of cell adhesion, causing a number of disease phenotypes, including cancer (12). In addition, loss of E-cadherin expression is often used as a marker for epithelial to mesenchymal transition and cancer progression (13, 14). E-cadherin is a type I transmembrane protein that exhibits fluid—albeit somewhat restricted—motion in the cell membrane (15–17). Cadherin adsorbed onto solid substrates is routinely used for in vitro cell studies (18–20). Although solid surface-adsorbed cadherin is capable of binding cadherin on an apposed cell surface, the imposed immobility precludes subsequent assembly into natural structures, and the functional consequences of this remain unclear.

Here, we reconstituted E-cadherin-mediated adhesion between living cells and E-cadherin extracellular domain (E-cad-ECD)-functionalized supported lipid bilayer membranes. This type of hybrid live cell-supported membrane platform has proven to be effective in reconstitution of other juxtacrine signaling systems, in which mobility and spatial assembly of receptors proved to enable important aspects of biological function that are lost in a solid display format (6–8, 21–23). We anticipate similar benefits when the system is applied to cadherins. Supported lipid bilayers allow control over the identity, density, and diffusional characteristics of protein molecules. Significantly, supported membranes also allow dynamic spatial assembly of

Significance

Epithelial (E)-cadherin-based adherens junctions are the basis of epithelial tissue integrity in Metazoans. They are composed of E-cadherin molecules interacting with each other from apposed cells. Using artificial supported lipid bilayers functionalized with the full-length extracellular domain of E-cadherin and live cells, we show that E-cadherin junction formation involves a nucleation process mediated by active filopodia retraction and requiring reduced mobility of E-cadherin on supported lipid bilayers. These results underscore the importance of controlling physical aspects of the cellular microenvironment with synthetic materials for in vitro live cell applications. In this case, tuning the mobility of a viscous fluid display surface enabled functional reconstitution of a cadherin-mediated adhesion junction.

Author contributions: K.H.B., K.L.H., C.-h.Y., A.W.S., M.L.D., L.S., B.H., R.Z.-B., and J.T.G. designed research; K.H.B., K.L.H., C.-h.Y., O.J.H., H.S., A.W.S., W.Y.C.H., W.-C.L., and Z.G. performed research; O.J.H., H.S., A.W.S., A.P., and S.M.T. contributed new reagents/analytic tools; K.H.B., K.L.H., C.-h.Y., A.W.S., W.Y.C.H., W.-C.L., R.Z.-B., and J.T.G. analyzed data; and K.H.B., K.L.H., A.W.S., S.M.T., M.L.D., L.S., B.H., R.Z.-B., and J.T.G. wrote the paper.

Reviewers: K.S., Centre Interdisciplinaire de Nanoscience de Marseille; and S.S., Iowa State University.

The authors declare no conflict of interest.

Freely available online through the PNAS open access option.

[1]K.H.B. and K.L.H. contributed equally to this work.

[2]Present address: School of Biomedical Sciences, Li Ka Shing Faculty of Medicine, The University of Hong Kong, Pok Fu Lam, Hong Kong.

[3]Present address: Department of Chemistry, University of Akron, Akron, OH 44325.

[4]To whom correspondence may be addressed. Email: bh6@cumc.columbia.edu, biezbr@nus.edu.sg, or jtgroves@lbl.gov.

This article contains supporting information online at www.pnas.org/lookup/suppl/doi:10.1073/pnas.1513775112/-/DCSupplemental.

extended structures, as can occur in a physiological situation, but which is not possible with proteins directly adsorbed onto solid substrates.

From the results presented here, it is evident that the mechanism of hybrid junction formation between cells and the E-cad-ECD supported membranes is a dynamic process involving active extension and retraction of filopodia. The resulting hybrid junctions exhibit enrichment of E-cad-ECD in the supported membrane, recruitment of α-catenin (the mechanosensory protein found in adherens junctions) to corresponding regions of the live cell membrane, and remodeled cortical actin. Experiments with chemical inhibitors confirm that junction formation requires actomyosin contraction. A mutation known to destabilize the E-cadherin *cis* interface present in both the cell surface and the bilayer bound species did not significantly impair junction formation; however, deletion of the intracellular domain from the cell surface E-cadherin completely eliminated this process.

A key practical realization from the results presented here is that junction formation proceeds with much greater efficiency using supported membrane lipid compositions with low mobility. Additionally, junction formation is essentially all or nothing. Once successfully initiated, junction formation progresses to completion. Reduced membrane mobility results in two primary physical consequences on cadherin: (*i*) higher resistive forces to actively driven motion and (*ii*) elongated timescales for diffusive dissipation of localized concentrations of E-cad-ECD on the bilayer. The all-or-nothing nature of junction formation combined with the observed sensitivity to supported membrane mobility and active cellular processes indicates an active nucleation step, which can be defeated if the supported membrane E-cadherin exhibits too much freedom of motion. Previous efforts to reconstitute cadherin in supported bilayers have used an Fc-conjugated extracellular domain of E-cadherin linked to the bilayer via either GPI or biotin–streptavidin interaction (24–26). As will be directly evidenced in the results presented here, these early efforts most likely did not achieve the nucleation threshold required to establish extended E-cadherin-mediated junctions.

Overall, E-cadherin is unique among the juxtacrine receptor–ligand systems that so far have been studied in detail in hybrid live cell-supported membrane junctions (7, 8, 27–30). Intermembrane E-cadherin adhesion does not appear to follow simple laws of mass action. That is, the rate of intermembrane bond formation does not exhibit proportionality to receptor concentration as is seen in other systems, even when considering the geometry and mechanics of the intermembrane junction (31–33). Rather, E-cadherin junction formation requires active nucleation before extensive adhesive junctions form. This may reflect a regulatory mechanism that helps to minimize uncontrolled cellular adhesion in vivo.

Results

Biophysical Characterization of E-cadherin on Supported Lipid Bilayers. The mature E-cadherin molecule contains five amino-terminal extracellular cadherin domains in tandem (EC1–5) with multiple Ca^{2+} binding sites, followed by a single transmembrane domain and an intracellular cytoplasmic carboxyl-terminal domain. Crystal structures have revealed two types of interactions between E-cadherin extracellular domains: a *trans* interaction formed by β-strand swapping between the EC1 domains of apposing E-cadherin molecules, and a *cis* interaction formed between regions in the EC1 and EC2 domains of adjacent E-cadherin molecules (34). Disruption of the *trans* interaction interface abrogates cell–cell adhesion whereas disruption of the *cis* interaction interface inhibits localization of E-cadherin to junctions, although *trans* interactions are still observed (34, 35). Further, the formation of *trans*-interacting dimers of E-cadherin is a two-step process involving the formation of an intermediate X-dimer structure, which then converts to the final strand-swapped dimer (36).

To allow for all of these potential interactions in the reconstituted system, the C-terminal His_{12} tagged full E-cad-ECD was expressed in HEK 293F cells and purified using a Ni^{2+}-chelating column (Fig. 1*A*). The construct was engineered to contain a single free Cys residue in the EC5 domain (Cys499 of the mature E-cadherin) (*SI Materials and Methods*), which was used for site-specific fluorescent labeling. The labeled protein eluted as a single peak in size exclusion chromatography (Fig. 1*B*).

Supported lipid bilayers were functionalized with fluorescently labeled E-cad-ECD via the kinetic-controlled Ni-nitrilotriacetic acid (NTA)-poly-His chelation (23, 37, 38). Fluorescence recovery after photobleaching (FRAP) experiments revealed large-scale lateral mobility of the membrane-coupled E-cad-ECD in bilayers prepared with 1,2-dioleoyl-*sn*-glycero-3-phosphocholine (DOPC) as the base lipid (Fig. 1*C*). Precise Z-scan fluorescence correlation spectroscopy (FCS) measurements (39) revealed lateral diffusion coefficients, D, around 1.6 ± 0.1 $\mu m^2/s$ and molecular densities in the range of ∼100–700 molecules per square micrometer across multiple independently prepared bilayers, depending on incubation conditions (Fig. 1*D*) (37). The diffusion coefficient of E-cad-ECD obtained here is typical of monomeric proteins bound to lipid molecules in supported lipid bilayers by the Ni-NTA His chelation (38, 40), although higher than reported values of E-cadherin on live cell membranes (0.002–0.036 $\mu m^2/s$) (15–17). The surface density of E-cad-ECD on lipid bilayers is comparable to that on livings cells ($2.5–16 \times 10^4$ molecules per cell, which translates to ∼80–500 molecules per square micrometer, assuming the cell to be a sphere with a diameter of 10 μm) (41).

E-cad-ECD on Supported Lipid Bilayers Is Monomeric. The oligomeric state of cell surface cadherins outside of junctions has not been established experimentally, although an interaction between E-cadherin has been proposed based on FRAP experiments on live cell membranes (42), and actin-delimited clusters of E-cadherin have been observed by superresolution imaging (43). A low affinity *cis* interaction observed in extracellular domain crystal

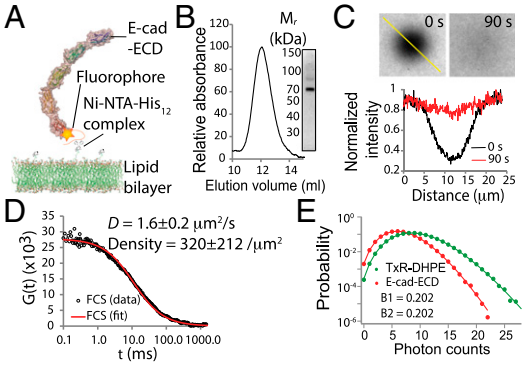

Fig. 1. Biophysical characterization of E-cad-ECD on supported lipid bilayers. (*A*) Schematic representation of E-cad-ECD bound to bilayer via Ni-NTA interaction. Relative position of the fluorophore on the crystal structure of the extracellular domain of E-cadherin (PDB: 3Q2V) is also shown. (*B*) Fluorescently labeled E-cad-ECD was subjected to size exclusion chromatography. *Inset* shows Coomassie stained SDS/PAGE image of E-cad-ECD. (*C*) FRAP analysis of E-cad-ECD functionalized lipid bilayer. (*Top*) Photobleached spot that recovers after 90 s. (*Bottom*) Line scan of the images. (*D*) FCS curve fit to a standard 2D, single-component diffusion model. Diffusion coefficient D and density shown in the box were determined from Z-scan FCS analysis of multiple E-cad-ECD containing bilayers. Values represent mean ± SD (*E*) PCH fit of an E-cad-ECD functionalized bilayer to a two-species model. Identical brightness of the two species obtained from the PCH fit, indicated as B1 and B2, shows that E-cad-ECD is present as single oligomeric species. PCH fit of TexasRed in TexasRed-DHPE containing bilayer is shown as a control.

structures and important for junctional localization could, in principle, allow E-cadherin to assemble into higher oligomeric states (34). FCS measurements of E-cad-ECD on supported lipid bilayers suggest a single diffusive species (Fig. 1*D*). However, the time autocorrelation function analysis used in FCS only provides average mobility information; it does not provide specific information on the distribution of oligomeric states. To resolve this, we performed photon counting histogram (PCH) analysis of the fluorescence intensity fluctuations. We have found PCH, which examines the time-independent brightness distribution of diffusing species, to be an accurate and reliable measure of stoichiometric heterogeneity of proteins on supported lipid bilayers (44). PCH measurements confirmed a single species of E-cad-ECD on the bilayer (Fig. 1*E*). The extremely low affinity of the *cis* interaction in solution ($K_d > 1$ mM in solution) and the formation of a continuous array of *cis*-interacting molecules seen in crystal structures and validated by mutagenesis (10, 34) essentially rule out the possibility that the single species found here is a dimer (45). Thus, E-cad-ECD is a monomer in the absence of *trans* interaction at surface densities similar to those observed in cells (41).

Interaction of Cells with E-cad-ECD Functionalized and Highly Fluid Supported Lipid Bilayers. We used the MKN-28 epithelial cell line to study E-cadherin junction formation in hybrid live cell-supported lipid bilayer format (Fig. 2*A*). These cells form closely packed colonies in culture and endogenously express E-cadherin and other crucial cell–cell adhesion proteins (46) (Fig. S1 *A* and *B*). In most cases, cells seeded on bilayers containing E-cad-ECD molecules showed no enrichment of the fluorescently labeled E-cad-ECD molecules attached to the bilayer. E-cad-ECD displayed on highly fluid surfaces ($D \geq 1$ μm^2/s) at physiological densities is essentially not competent for adhesion (see *SI Text* for other control experiments and Fig. S2).

However, in less than 1% of cases, strong enrichment and extensive junction formation was observed (Fig. 2*B*, Fig. S3. and Movie S1). Notably, weak or significantly impaired junctions were not observed. The process is essentially all or nothing: Once junction formation is successfully initiated, it goes to completion. This observation suggests that some sort of nucleation event is essential, but is not well reconstituted with the highly fluid supported membrane. We note that adhesion observed in early studies on live cells (26) or giant unilamellar vesicles (47, 48) and supported membranes did not resemble the extensive junction formation we report here, and we suggest that those systems failed to achieve the previously unknown nucleation step described here.

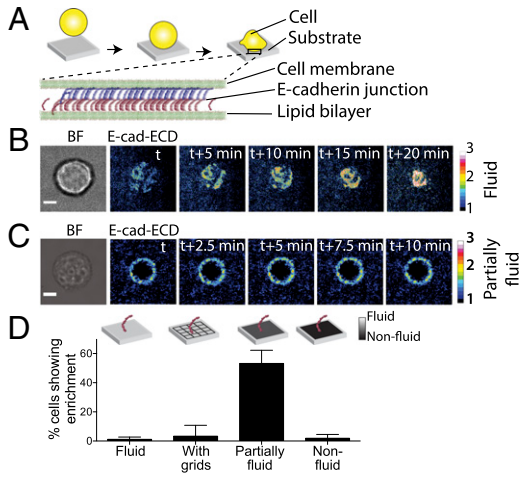

Fig. 2. E-cadherin mediated cell-bilayer junction formation. (*A*) Schematic representation of E-cadherin-mediated hybrid cell–bilayer junction formation. (*B* and *C*) Representative time series of epifluorescence images of E-cad-ECD showing enrichment of E-cad-ECD by MKN-28 cells on either fluid (*B*) or partially fluid (*C*) bilayers. Color bars represent fold increase in E-cad-ECD surface density. (Scale bar, 5 μm.) (*D*) Percentage of MKN28 cells showing E-cadherin enrichment on bilayers with different properties. Values represent mean ± SD from multiple experiments. *Inset* is a schematic representation of bilayer fluidity in gray scale.

E-cadherin Junctions Form Efficiently with Low-Mobility Supported Lipid Bilayers. Unlike the supported bilayer system where E-cadherin exhibits high diffusive mobility, E-cadherin on the surface of live cells exhibits reduced mobility, with a fraction of molecules confined laterally (15, 43, 49). We, therefore, attempted to systematically test if altering E-cad-ECD mobility on bilayers could increase the probability of junction nucleation and formation.

We manipulated the mobility of E-cad-ECD in supported lipid bilayers in two different ways. In the first approach, supported lipid bilayers were formed on substrates that were prepatterned with grids of metal lines ranging from 0.5 μm to 4 μm in spacing (7, 8, 50). In this configuration, local mobility of the E-cad-ECD within individual corrals is unchanged, while long-range transport across substrate-imposed barriers is blocked. However, confining E-cad-ECD on metal grids failed to induce cells to efficiently form junctions (Fig. 2*D*).

In the second approach, membrane composition was manipulated to uniformly increase the average viscosity of the membrane. E-cad-ECD displayed on low-mobility bilayers prepared using 1,2-dipalmitoyl-*sn*-glycero-3-phosphocholine (DPPC) doped with either 0.1 or 1 mole % acyl chain labeled 1-acyl-2-[12-[(7-nitro-2-1,3-benzoxadiazol-4-yl)amino]dodecanoyl]-sn-glycero-3-phosphocholine (NBD-PC) and 4 mole % 1,2-dioleoyl-*sn*-glycero-3-[(N-(5-amino-1-carboxypentyl)iminodiacetic acid)succinyl] nickel salt (Ni-NTA-DOGS) enabled cells to form junctions efficiently (Fig. 2 *C* and *D*). The bulky fluorescent NBD group at the C12 position in the acyl chain of the phosphatidylcholine is known to disrupt molecular ordering, and thus reduce the melting temperature of DPPC bilayers (51); these membranes are not in a fully gel phase at the experimental temperature (37 °C) and are not expected to be phase separated due to the low density of Ni-NTA-DOGS used. FRAP experiments on these bilayers allowed an estimation of the diffusion coefficient of 0.04 μm^2/s for the NBD-PC lipid molecules (Fig. S4). However, E-cad-ECD on the same bilayer did not show a significant recovery even after 30 min of bleaching (Figs. S4 and S5), indicating an even lower effective mobility, which may overlap with the range of reported apparent diffusion coefficients of E-cadherin on live cell membranes (0.002–0.036 μm^2/s) (15–17). It is important to realize that for membrane systems with such low mobility, the diffusion coefficient is not generally a well-defined physical parameter. Clustering, frictional coupling, and interactions with fixed obstacles all contribute to the effective mobility (52–59). We note that although E-cad-ECD on these bilayers does not show diffusive motion, they are not immobilized on the surface. Thus, application of force by living cells resulted in some rearrangement of E-cad-ECD on these bilayers, which was not seen with bilayers containing only DPPC (gel state under experimental conditions) and 4 mole % Ni-NTA-DOGS at 37 °C (Fig. 2*D*). The difference in the morphologies of E-cadherin junctions formed on these and the fluid DOPC bilayers (see Fig. 2*B*) was due to the difference in the diffusive mobility of the *trans*-interacting molecules. That is, when cells manage to start a junction on a fluid membrane, the already adhered cadherin continues to move around freely and, therefore, fill the interior of the junction (Movie S1).

Reduction of the intrinsic mobility of E-cadherin creates two distinct physical effects. First, any actively driven transport of cadherin is met by larger opposing forces (*SI Text*) (60), and thus could conceivably activate a force-sensitive catch bond or mechanosensory system. Single-molecule experiments suggesting

force-dependent catch bond formation by a mutant E-cadherin that forms the intermediate X-dimer have been reported; however, no such catch bond has been observed for the wild type E-cadherin construct used in the experiments we report here (61). Second, the timescale for diffusive dissipation of any localized concentration of cadherin is elongated. As will be detailed below, this is directly visible in our experiments. Thus, local concentration-mediated kinetic nucleation of stable intermembrane E-cadherin interaction appears to play a role in junction formation.

Both cellular E-cadherin and α-catenin were found to colocalize with enriched zones of E-cad-ECD on the bilayer, and successful junction formation required Ca^{2+} (Fig. 3 *A* and *B*). Phalloidin staining of cells revealed a cortical actin ring around zones of E-cad-ECD enrichment, which is a characteristic of adherens junctions between living cells (62) (Fig. 3*E*). Similar results were observed in the rare cases where cells formed junctions on fluid bilayers, suggesting that once nucleated, the cadherin junction is no longer sensitive to membrane lipid mobility (Fig. S6*C*).

Active Cytoskeletal Processes Are Required for Cell–Cell Junction Formation. Active filopodia extension and retraction were clearly visible by reflection interference contrast microscopy (RICM) during junction formation on the supported bilayers. Additionally, localized concentrations of E-cad-ECD occurred under these filopodia and could be seen to move back toward the cell periphery along with filopodia retraction (Fig. 4*A* and Movie S2). Pretreatment of cells with a Cdc42 inhibitor (ML 141) resulted in a loss of filopodia and the E-cad-ECD enrichment (Fig. 4*B* and Fig. S6*D*). Pretreatment of cells with blebbistatin, which is an inhibitor of myosin II, or with antimycin A in combination with 2'-deoxy glucose, which deplete ATP, also reduced the frequencies of cells forming junctions (Fig. 4*B*). In contrast, treatment of cells with calyculin A (63), a phosphatase inhibitor that increases the cellular actomyosin contractility (64), resulted in an increase in the frequency of successful junction formation (Fig. 4*B*).

The Intracellular Domain of E-Cadherin, but Not the *cis* Interaction, Is Essential to Initiate Junction Formation. Structural studies have revealed a *cis* interface between the E-cadherin monomers from the same cell, and ablation of the *cis* interaction by site-directed mutagenesis (V81D L175D) has been found to significantly alter the ordering and dynamics of E-cadherin clustering and

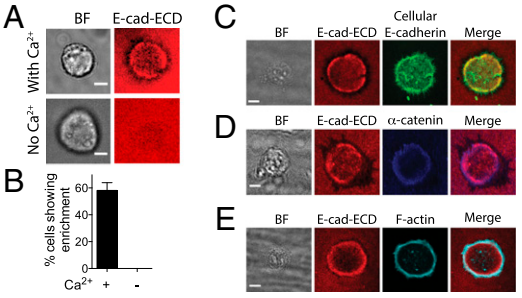

Fig. 3. Characterization of hybrid cell–bilayer junctions. (*A*) Bright field images of MKN28 cells seeded on partially fluid bilayers functionalized with E-cad-ECD in the presence or absence of Ca^{2+} and epifluorescence images of E-cad-ECD on bilayers showing the formation or lack of a junction. (*B*) Percentage of MKN28 cells showing E-cad-ECD enrichment on partially fluid bilayers in the presence or absence of Ca^{2+}. Values represent mean ± SD from multiple experiments. (Scale bar, 5 μm.) (*C*–*E*) MKN-28 cells forming junctions on partially fluid bilayers were either immunostained for cellular E-cadherin using an antibody raised against the intracellular part of E-cadherin (*C*) and an antibody against α-catenin (*D*) or stained with phalloidin (*E*). Cellular E-cadherin and α-catenin colocalize with E-cad-ECD molecules on bilayer whereas F-actin is remodeled to form a ring around the hybrid junction. (Scale bar, 5 μm.)

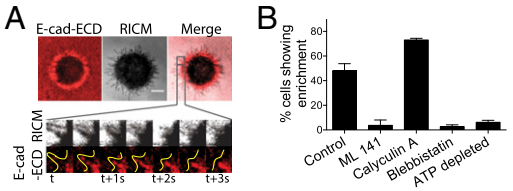

Fig. 4. E-cadherin clustering and junction formation is an actomyosin-dependent process. (*A*) Epifluorescence and RICM imaging of the cell shown in Fig. 2*C* revealing a tight contact with the bilayer around the zone of E-cad-ECD enrichment. Zoomed-in view of a retracting filopodia shows clustering of E-cad-ECD molecules. A trace of the retracting filopodia is overlapped on the epifluorescence image of E-cad-ECD on the bilayer. Numbers indicate time in minutes, with initial time assumed to be *t*. (*B*) Percentage of MKN28 cells, either untreated or treated with ML 141, calyculin A, blebbistatin, or a combination of antimycin A and 2′-deoxy glucose, showing enrichment of E-cad-ECD on partially fluid bilayers. Values represent mean ± SD from multiple experiments. (Scale bar, 5 μm.)

localization of E-cadherin to adherens junctions (34, 35). To test the role of the *cis* interface in the nucleation of E-cadherin, we used the cadherin-negative variant of the E-cad expressing A-431 epithelial cells, denoted A-431D (34, 65). A-431D cells expressing the *cis*-mutant E-cadherin seeded on low-mobility bilayers functionalized with the *cis*-mutant E-cad-ECD showed a similar frequency of junction formation as was found with A-431D cells expressing wild-type E-cadherin on wild-type E-cad-ECD functionalized low-mobility bilayers (Fig. 5*A* and Fig. S6*E*), suggesting that the *cis* interaction is not necessary for the formation of junction-like structures in these bilayer assays. We note that this lack of difference in the frequency of junction formation is not a result of a difference in the expression levels of the wild-type and *cis*-mutant E-cadherin, as these cells express the proteins at similar levels (35).

The intracellular domain of E-cadherin both regulates various signaling proteins by its multiple interaction sites and forms a linkage with the actin cytoskeleton through β- and α-catenins, as well as other proteins (42, 66–70). This link has been suggested to stabilize cadherin *cis* interactions, thereby stabilizing the entire cadherin adhesive structure (35). However, the intracellular domain is not essential for the formation of some junction-like structures as cells expressing only the extracellular domain form such structures, which depend on both the *cis* and *trans* interaction interfaces of E-cadherin (43, 65). How exactly the intracellular domain of E-cadherin and its interaction with the cytoskeleton cooperate with the extracellular domain of E-cadherin in the process of junction formation is not completely understood.

We tested the role of the intracellular domain of E-cadherin in junction formation by comparing wild-type E-cadherin with its cytoplasmic domain-deleted mutant. Unlike A-431D cells expressing wild-type E-cadherin that formed junctions, A-431D cells expressing the intracellular domain-deleted E-cadherin with an intact extracellular domain failed to form junctions on partially fluid bilayers (Fig. 5*A* and Fig. S6*E*) (34, 65).

The fact that the intracellular domain-deleted E-cadherin failed to form junctions raised the possibility that E-cadherin engagement with the actin cytoskeleton is required for junction formation. It is possible that the low frequency of junction formation on the fluid bilayers is caused by inability of cells in this condition to appropriately interconnect cadherin with the actin cytoskeleton. To test this possibility, we characterized junction formation by MKN28 cells expressing a fusion protein containing the actin-binding domain of α-catenin fused to the C terminus of E-cadherin (Fig. S6*G*). This strategy has been used previously to constitutively link E-cadherin to the actin cytoskeleton (35, 71). However, even such direct engagement of E-cadherin with the

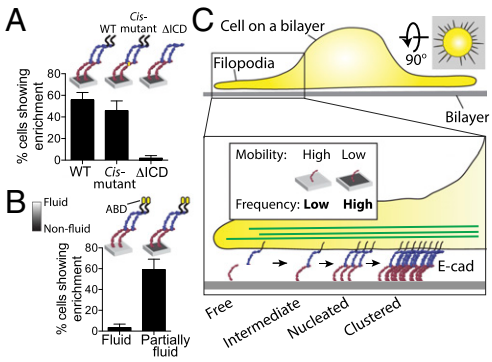

Fig. 5. Mechanism of E-cadherin junction formation. (*A*, *Bottom*) Percentage of A-431D cells expressing wild-type, *cis*-mutant, or intracellular domain-deleted E-cadherin showing enrichment of fluorescently labeled E-cad-ECD on partially fluid bilayers functionalized with wild-type, *cis*-mutant, or wild-type E-cad-ECD, respectively. (*Top*) Schematic representation of junction formation by wild-type, *cis*-mutant, or intracellular domain-deleted E-cadherin on partially fluid bilayers. (*B*, *Bottom*) Percentage of MKN28 cells expressing E-cadherin fused with the actin-binding domain of α-catenin showing E-cad-ECD enrichment on fluid or partially fluid bilayers functionalized with the wild-type E-cad-ECD. (*Top*) Schematic representation of junction formation by E-cadherin fused to the actin-binding domain of α-catenin on fluid and partially fluid bilayers. Values represent mean ± SD from multiple experiments. (Scale bar, 5 μm.) (*C*) Schematic representation of E-cadherin junction formation on a supported lipid bilayer involving filopodia retraction-mediated local increase in E-cad-ECD concentration.

actin cytoskeleton did not increase the frequency of junction formation on fluid bilayers (Fig. 5*B* and Fig. S6*F*).

Conclusion

Based on the composite of observations described above, we propose the following mechanism for E-cadherin junction formation in the hybrid live cell-supported membrane system (Fig. 5*C*). Junction formation is an active process requiring actomyosin-driven extension and retraction of filopodia. Cellular E-cadherin molecules interact with the actin cytoskeleton via the intracellular domain and are enriched in the dense F-actin networks present in the filopodia (70). E-cadherin molecules present on the surface of the filopodia interact with bilayer bound E-cadherin, resulting in the formation of the intermediate cadherin–cadherin bond (36). Localized increase in the concentration of the cadherin is achieved as bound cadherin are dragged back, and laterally compressed, with the retracting filopodium. On a liquid-disordered bilayer displaying high-mobility E-cadherin, this localized concentration of the E-cadherin dissipates too quickly by diffusion, even in the presence of an intact *cis* interaction interface, to enable development of the stable strand-swapped dimer needed for stable *trans* interactions. In contrast to this, local enrichments of E-cad-ECD in low-mobility supported membranes are dissipated much more slowly, thus enabling efficient formation of the stable strand-swapped dimer and clustering. A longer interaction time achieved in these low-mobility bilayers may allow E-cadherin to convert to the stable, strand-swapped *trans* dimer in a way that was seen in single-molecule force spectroscopy experiments (61). However, failure of the cells to form junctions when filopodia formation is inhibited (Fig. 4*B*) suggests that this may not be the sole factor controlling the frequency of cell–bilayer junction formation. Kinetic stabilization provided by the low-mobility supported membrane is sufficient to overcome the need for *cis* interactions. However, the junctions formed with the *cis*-mutant E-cadherin may not be assembled into 2D lattices as seen in cell–cell interfaces but, rather, may represent a concentrated assembly driven entirely by *trans* interactions. We speculate that subtle differences in the mobility of free cadherin on the cell surface, along with competition from other cell surface molecules, may create a reaction environment where the added effects of *cis* interactions are required for junction formation.

Materials and Methods

Full details are available in *SI Materials and Methods*. Briefly, wild-type or V81D L175D *cis*-mutant (34) E-cad-ECD (domains EC1–5 comprising residues Asp1 to Asp533 of the mature, furin-processed protein) engineered to contain a single cysteine residue were expressed and purified from HEK293 cells, and site-specifically labeled with fluorescent dye to observe junction formation. All bilayers were prepared using vesicle fusion method (40). Bilayers were functionalized with proteins via Ni-NTA-poly-His chelation (37). FRAP was performed by illuminating a small field of view (15–30 μm diameter) at high intensity followed by continued imaging to observe recovery of fluorescence. FCS was performed by illuminating a diffraction-limited spot using a pulsed super continuum laser (SuperK Extreme; NKT Photonics) bilayers through a 100× oil objective, and data were analyzed using homebuilt codes in Matlab. Hybrid cell–bilayer junctions were reconstituted by seeding cadherin-expressing cells on bilayers, and enrichment of E-cad-ECD fluorescence on the bilayer was observed by epifluorescence. Frequency of junction formation was determined manually. Substrates with chromium grids were prepared by nanoimprinting (7). Diffusion of E-cad-ECD on bilayers was reduced by changing the constituent lipid compositions from DOPC to DPPC+NBD-PC. Cells were stained with specific antibodies or phalloidin and imaged by confocal microscopy to confirm the composition of junctions. Cells were treated with ML 141 to inhibit filopodia formation, calyculin A to increase and blebbistatin to decrease actomyosin tension, and a combination of 2′-deoxy glucose and antimycin A to deplete ATP in cells. A431-D cells expressing wild-type, cis-mutant, and intracellular domain-deleted mutant have been previously described (34, 65). FRAP, FCS, and imaging were performed with a 100× objective in an Eclipse Ti inverted microscope (Nikon).

ACKNOWLEDGMENTS. This work was supported by National Research Foundation (NRF) through the Mechanobiology Institute, National University of Singapore and NRF Competitive Research Programme (CRP) Grant CRP001-084. R.Z.-B. was supported by the National Research Foundation Singapore under its NRF fellowship (NRF-RF2009-RF001-074). M.L.D. was supported by the National Institutes of Health (AI043542) and a Principal Research fellowship (100262/Z/12/Z) funded by the Wellcome Trust and the Kennedy Trust for Rheumatology. This work was also supported in part by the US National Institutes of Health (R01 GM062270 to L.S. and AR44016 to S.M.T.) and the National Science Foundation (MCB-1412472 to B.H.).

1. Chen CS, Mrksich M, Huang S, Whitesides GM, Ingber DE (1997) Geometric control of cell life and death. *Science* 276(5317):1425–1428.
2. Boudreau N, Sympson CJ, Werb Z, Bissell MJ (1995) Suppression of ICE and apoptosis in mammary epithelial cells by extracellular matrix. *Science* 267(5199): 891–893.
3. Nelson CM, Vanduijn MM, Inman JL, Fletcher DA, Bissell MJ (2006) Tissue geometry determines sites of mammary branching morphogenesis in organotypic cultures. *Science* 314(5797):298–300.
4. Engler AJ, Sen S, Sweeney HL, Discher DE (2006) Matrix elasticity directs stem cell lineage specification. *Cell* 126(4):677–689.
5. Levental KR, et al. (2009) Matrix crosslinking forces tumor progression by enhancing integrin signaling. *Cell* 139(5):891–906.
6. Manz BN, Jackson BL, Petit RS, Dustin ML, Groves J (2011) T-cell triggering thresholds are modulated by the number of antigen within individual T-cell receptor clusters. *Proc Natl Acad Sci USA* 108(22):9089–9094.
7. Salaita K, et al. (2010) Restriction of receptor movement alters cellular response: Physical force sensing by EphA2. *Science* 327(5971):1380–1385.
8. Mossman KD, Campi G, Groves JT, Dustin ML (2005) Altered TCR signaling from geometrically repatterned immunological synapses. *Science* 310(5751):1191–1193.
9. Patel SD, Chen CP, Bahna F, Honig B, Shapiro L (2003) Cadherin-mediated cell-cell adhesion: Sticking together as a family. *Curr Opin Struct Biol* 13(6):690–698.
10. Brasch J, Harrison OJ, Honig B, Shapiro L (2012) Thinking outside the cell: How cadherins drive adhesion. *Trends Cell Biol* 22(6):299–310.
11. Troyanovsky S (2012) Adherens junction assembly. *Subcell Biochem* 60:89–108.
12. Vasioukhin V (2012) Adherens junctions and cancer. *Subcell Biochem* 60:379–414.
13. Kowalski PJ, Rubin MA, Kleer CG (2003) E-cadherin expression in primary carcinomas of the breast and its distant metastases. *Breast Cancer Res* 5(6):R217–R222.
14. Singhai R, et al. (2011) E-Cadherin as a diagnostic biomarker in breast cancer. *N Am J Med Sci* 3(5):227–233.
15. Adams CL, Chen YT, Smith SJ, Nelson WJ (1998) Mechanisms of epithelial cell–cell adhesion and cell compaction revealed by high-resolution tracking of E-cadherin-green fluorescent protein. *J Cell Biol* 142(4):1105–1119.
16. Sako Y, Nagafuchi A, Tsukita S, Takeichi M, Kusumi A (1998) Cytoplasmic regulation of the movement of E-cadherin on the free cell surface as studied by optical tweezers

and single particle tracking: Corralling and tethering by the membrane skeleton. *J Cell Biol* 140(5):1227–1240.
17. Kusumi A, Sako Y, Yamamoto M (1993) Confined lateral diffusion of membrane receptors as studied by single particle tracking (nanovid microscopy). Effects of calcium-induced differentiation in cultured epithelial cells. *Biophys J* 65(5):2021–2040.
18. Gavard J, et al. (2004) Lamellipodium extension and cadherin adhesion: Two cell responses to cadherin activation relying on distinct signalling pathways. *J Cell Sci* 117(Pt 2):257–270.
19. Ladoux B, et al. (2010) Strength dependence of cadherin-mediated adhesions. *Biophys J* 98(4):534–542.
20. Ganz A, et al. (2006) Traction forces exerted through N-cadherin contacts. *Biol Cell* 98(12):721–730.
21. Grakoui A, et al. (1999) The immunological synapse: A molecular machine controlling T cell activation. *Science* 285(5425):221–227.
22. O'Donoghue GP, Pielak RM, Smoligovets AA, Lin JJ, Groves JT (2013) Direct single molecule measurement of TCR triggering by agonist pMHC in living primary T cells. *eLife* 2:e00778.
23. Hartman NC, Nye JA, Groves JT (2009) Cluster size regulates protein sorting in the immunological synapse. *Proc Natl Acad Sci USA* 106(31):12729–12734.
24. Andreasson-Ochsner M, et al. (2011) Single cell 3-D platform to study ligand mobility in cell-cell contact. *Lab Chip* 11(17):2876–2883.
25. Charnley M, Kroschewski R, Textor M (2012) The study of polarisation in single cells using model cell membranes. *Integr Biol (Camb)* 4(9):1059–1071.
26. Perez TD, Nelson WJ, Boxer SG, Kam L (2005) E-cadherin tethered to micropatterned supported lipid bilayers as a model for cell adhesion. *Langmuir* 21(25):11963–11968.
27. Pautot S, Lee H, Isacoff EY, Groves JT (2005) Neuronal synapse interaction reconstituted between live cells and supported lipid bilayers. *Nat Chem Biol* 1(5):283–289.
28. Liu D, Peterson ME, Long EO (2012) The adaptor protein Crk controls activation and inhibition of natural killer cells. *Immunity* 36(4):600–611.
29. Yokosuka T, et al. (2012) Programmed cell death 1 forms negative costimulatory microclusters that directly inhibit T cell receptor signaling by recruiting phosphatase SHP2. *J Exp Med* 209(6):1201–1217.
30. Dustin ML, Ferguson LM, Chan PY, Springer TA, Golan DE (1996) Visualization of CD2 interaction with LFA-3 and determination of the two-dimensional dissociation constant for adhesion receptors in a contact area. *J Cell Biol* 132(3):465–474.
31. Qi SY, Groves JT, Chakraborty AK (2001) Synaptic pattern formation during cellular recognition. *Proc Natl Acad Sci USA* 98(12):6548–6553.
32. Weikl TR, Groves JT, Lipowsky R (2002) Pattern formation during adhesion of multicomponent membranes. *Europhys Lett* 59(6):916–922.
33. Hu J, Lipowsky R, Weikl TR (2013) Binding constants of membrane-anchored receptors and ligands depend strongly on the nanoscale roughness of membranes. *Proc Natl Acad Sci USA* 110(38):15283–15288.
34. Harrison OJ, et al. (2011) The extracellular architecture of adherens junctions revealed by crystal structures of type I cadherins. *Structure* 19(2):244–256.
35. Hong S, Troyanovsky RB, Troyanovsky SM (2013) Binding to F-actin guides cadherin cluster assembly, stability, and movement. *J Cell Biol* 201(1):131–143.
36. Harrison OJ, et al. (2010) Two-step adhesive binding by classical cadherins. *Nat Struct Mol Biol* 17(3):348–357.
37. Nye JA, Groves JT (2008) Kinetic control of histidine-tagged protein surface density on supported lipid bilayers. *Langmuir* 24(8):4145–4149.
38. Xu Q, Lin WC, Petit RS, Groves JT (2011) EphA2 receptor activation by monomeric Ephrin-A1 on supported membranes. *Biophys J* 101(11):2731–2739.
39. Humpolíková J, et al. (2006) Probing diffusion laws within cellular membranes by Z-scan fluorescence correlation spectroscopy. *Biophys J* 91(3):L23–L25.
40. Lin WC, Yu CH, Triffo S, Groves JT (2010) Supported membrane formation, characterization, functionalization, and patterning for application in biological science and technology. *Curr Protoc Chem Biol* 2(4):235–269.
41. Duguay D, Foty RA, Steinberg MS (2003) Cadherin-mediated cell adhesion and tissue segregation: Qualitative and quantitative determinants. *Dev Biol* 253(2):309–323.
42. Yamada S, Pokutta S, Drees F, Weis WI, Nelson WJ (2005) Deconstructing the cadherin-catenin-actin complex. *Cell* 123(5):889–901.
43. Wu Y, Kanchanawong P, Zaidel-Bar R (2015) Actin-delimited adhesion-independent clustering of E-cadherin forms the nanoscale building blocks of adherens junctions. *Dev Cell* 32(2):139–154.
44. Lin WC, et al. (2014) H-Ras forms dimers on membrane surfaces via a protein–protein interface. *Proc Natl Acad Sci USA* 111(8):2996–3001.
45. Wu Y, Vendome J, Shapiro L, Ben-Shaul A, Honig B (2011) Transforming binding affinities from three dimensions to two with application to cadherin clustering. *Nature* 475(7357):510–513.
46. Guo Z, et al. (2014) E-cadherin interactome complexity and robustness resolved by quantitative proteomics. *Sci Signal* 7(354):rs7.
47. Puech PH, Feracci H, Brochard-Wyart F (2004) Adhesion between giant vesicles and supported bilayers decorated with chelated E-cadherin fragments. *Langmuir* 20(22):9763–9768.
48. Fenz SF, Merkel R, Sengupta K (2009) Diffusion and intermembrane distance: Case study of avidin and E-cadherin mediated adhesion. *Langmuir* 25(2):1074–1085.
49. Perez TD, Tamada M, Sheetz MP, Nelson WJ (2008) Immediate-early signaling induced by E-cadherin engagement and adhesion. *J Biol Chem* 283(8):5014–5022.
50. Groves JT, Ulman N, Boxer SG (1997) Micropatterning fluid lipid bilayers on solid supports. *Science* 275(5300):651–653.
51. Loura LM, Fernandes F, Fernandes AC, Ramalho JP (2008) Effects of fluorescent probe NBD-PC on the structure, dynamics and phase transition of DPPC. A molecular dynamics and differential scanning calorimetry study. *Biochim Biophys Acta* 1778(2):491–501.
52. Kaizuka Y, Groves JT (2004) Structure and dynamics of supported intermembrane junctions. *Biophys J* 86(2):905–912.
53. Forstner MB, Yee CK, Parikh AN, Groves JT (2006) Lipid lateral mobility and membrane phase structure modulation by protein binding. *J Am Chem Soc* 128(47):15221–15227.
54. Lohmüller T, Xu Q, Groves JT (2013) Nanoscale obstacle arrays frustrate transport of EphA2-Ephrin-A1 clusters in cancer cell lines. *Nano Lett* 13(7):3059–3064.
55. Caculitan NG, et al. (2014) Size-based chromatography of signaling clusters in a living cell membrane. *Nano Lett* 14(5):2293–2298.
56. Ziemba BP, Falke JJ (2013) Lateral diffusion of peripheral membrane proteins on supported lipid bilayers is controlled by the additive frictional drags of (1) bound lipids and (2) protein domains penetrating into the bilayer hydrocarbon core. *Chem Phys Lipids* 172-173:67–77.
57. Knight JD, Lerner MG, Marcano-Velázquez JG, Pastor RW, Falke JJ (2010) Single molecule diffusion of membrane-bound proteins: Window into lipid contacts and bilayer dynamics. *Biophys J* 99(9):2879–2887.
58. He HT, Marguet D (2011) Detecting nanodomains in living cell membrane by fluorescence correlation spectroscopy. *Annu Rev Phys Chem* 62:417–436.
59. Kusumi A, et al. (2012) Membrane mechanisms for signal transduction: The coupling of the meso-scale raft domains to membrane-skeleton-induced compartments and dynamic protein complexes. *Semin Cell Dev Biol* 23(2):126–144.
60. Weber J (1956) Fluctuation dissipation theorem. *Phys Rev* 101(6):1620–1626.
61. Rakshit S, Zhang Y, Manibog K, Shafraz O, Sivasankar S (2012) Ideal, catch, and slip bonds in cadherin adhesion. *Proc Natl Acad Sci USA* 109(46):18815–18820.
62. Zhang J, et al. (2005) Actin at cell–cell junctions is composed of two dynamic and functional populations. *J Cell Sci* 118(Pt 23):5549–5562.
63. Ishihara H, et al. (1989) Calyculin A and okadaic acid: Inhibitors of protein phosphatase activity. *Biochem Biophys Res Commun* 159(3):871–877.
64. Henson JH, et al. (2003) Actin-based centripetal flow: Phosphatase inhibition by calyculin-A alters flow pattern, actin organization, and actomyosin distribution. *Cell Motil Cytoskeleton* 56(4):252–266.
65. Hong S, Troyanovsky RB, Troyanovsky SM (2010) Spontaneous assembly and active disassembly balance adherens junction homeostasis. *Proc Natl Acad Sci USA* 107(8):3528–3533.
66. Wheelock MJ, Johnson KR (2003) Cadherin-mediated cellular signaling. *Curr Opin Cell Biol* 15(5):509–514.
67. McEwen AE, Escobar DE, Gottardi CJ (2012) Signaling from the adherens junction. *Subcell Biochem* 60:171–196.
68. Drees F, Pokutta S, Yamada S, Nelson WJ, Weis WI (2005) Alpha-catenin is a molecular switch that binds E-cadherin-beta-catenin and regulates actin-filament assembly. *Cell* 123(5):903–915.
69. Zaidel-Bar R (2013) Cadherin adhesome at a glance. *J Cell Sci* 126(Pt 2):373–378.
70. Ratheesh A, Yap AS (2012) A bigger picture: Classical cadherins and the dynamic actin cytoskeleton. *Nat Rev Mol Cell Biol* 13(10):673–679.
71. Ozono K, Komiya S, Shimamura K, Ito T, Nagafuchi A (2011) Defining the roles of α-catenin in cell adhesion and cytoskeleton organization: Isolation of F9 cells completely lacking cadherin-catenin complex. *Cell Struct Funct* 36(1):131–143.
72. Yu CH, Law JB, Suryana M, Low HY, Sheetz MP (2011) Early integrin binding to Arg-Gly-Asp peptide activates actin polymerization and contractile movement that stimulates outward translocation. *Proc Natl Acad Sci USA* 108(51):20585–20590.
73. Endres NF, et al. (2013) Conformational coupling across the plasma membrane in activation of the EGF receptor. *Cell* 152(3):543–556.
74. Triffo SB, Huang HH, Smith AW, Chou ET, Groves JT (2012) Monitoring lipid anchor organization in cell membranes by PIE-FCCS. *J Am Chem Soc* 134(26):10833–10842.
75. Groves JT, Parthasarathy R, Forstner MB (2008) Fluorescence imaging of membrane dynamics. *Annu Rev Biomed Eng* 10:311–338.
76. Kametani Y, Takeichi M (2007) Basal-to-apical cadherin flow at cell junctions. *Nat Cell Biol* 9(1):92–98.
77. Delanoë-Ayari H, Al Kurdi R, Vallade M, Gulino-Debrac D, Riveline D (2004) Membrane and acto-myosin tension promote clustering of adhesion proteins. *Proc Natl Acad Sci USA* 101(8):2229–2234.

Supporting Information

Biswas et al. 10.1073/pnas.1513775112

SI Materials and Methods

Expression, Purification, and Fluorescent Labeling of E-cad-ECD. The cDNA encoding the extracellular region of mouse E-cadherin (domains EC1–5 comprising residues Asp1 to Asp533 of the mature, furin-processed protein) with a C-terminal 12×His purification tag and a human CD33 signal sequence replacing the native signal peptide and prodomain was inserted into the *Hind*III and NotI sites of the mammalian expression vector pCEP4 (Life Technologies). To produce a construct containing only a single cysteine in the extracellular region for labeling, Cys9 in EC1 and Cys532 in EC5 were mutated to serine with a QuikChange mutagenesis kit (Agilent Technologies). The single remaining cysteine residue at position 449 in the A strand of domain EC5, which normally forms a disulfide linkage in the native protein with Cys534 that is not included in the construct expressed here, is available for labeling with sulfhydryl-reactive dyes. The construct was introduced into HEK-293F cells using Lipofectamine 2000 (Life Technologies), and transfectants were selected with 200 μg/mL hygromycin-B (Mediatech) in DMEM:F12 supplemented with 10% fetal calf serum. Secreted His-tagged E-cadherin extracellular regions were collected from 2–4 L of conditioned media by Ni-NTA affinity chromatography in a batch procedure (3 h, 25 °C), and were further purified by anion and cation exchange and size exclusion chromatography using an Akta FPLC system (GE Healthcare). For fluorescent labeling, purified proteins at a concentration of ∼1 mg/mL were dialyzed into buffer containing 150 mM NaCl, 0.25 M Hepes pH 7.0, and 3 mM $CaCl_2$ and incubated with a ∼20-fold molar excess of sulfhydryl-specific Alexa Fluor 568 C5-maleimide (Life Technologies) for 5 h at 25 °C. Excess dye was removed by gel filtration, and the final labeled protein was concentrated to 1–2 mg/mL in 150 mM NaCl, 20 mM Bis-Tris pH 6.0, and 3 mM $CaCl_2$. Labeling efficiencies of ∼50–70% were obtained. A mutant E-cad-ECD containing V81D L175D described previously (34) was also purified and labeled in a similar way. EphrinA1-EYFP was purified essentially as described previously (38).

Supported Lipid Bilayer Preparation. Supported lipid bilayers were prepared as described previously (40). Chloroform solutions of either DOPC or DPPC were mixed with 4 mole % of 1,2-dioleoyl-*sn*-glycero-3-[(*N*-(5-amino-1-carboxypentyl)iminodiacetic acid)-succinyl] nickel salt (Ni-NTA-DOGS). Partially fluid DPPC bilayers prepared by addition of various concentrations of 1-acyl-2-[12-[(7-nitro-2–1,3-benzoxadiazol-4-yl)amino]dodecanoyl]-sn-glycero-3-phosphocholine (NBD-PC) were added to the vesicle preparations. Marina Blue-1,2-dihexadecanoyl-sn-glycero-3-phosphoethanolamine (Marina Blue-DHPE) purchased from Life Technologies was added to the vesicle preparations at a concentration of 1 mole % to visualize lipid coverage and fluidity in some experiments; 1,2-dipalmitoyl-sn-glycero-3-phosphoethanolamine-*N*-(cap biotinyl) (16:0 biotinyl-Cap-PE) at 0.2 mole %, Ni-NTA-DOGS at 3.8 mole %, and DOPC at 96 mole % was used for experiments with E-cad-ECD and RGD. Biotinylated RGD was anchored to biotinyl-Cap-PE via Cascade blue Neutravidin (Life Technologies). All lipids, unless stated otherwise, were purchased from Avanti Polar Lipids.

The chloroform mixtures were dried in a rotary evaporator, resulting in the formation of a thin lipid film, which was then hydrated with 2 mL of deionized water. The film was resuspended in water, either by pipetting or overnight incubation at 4 °C, resulting in a final lipid concentration of 0.5 mg/mL. Keeping the solution chilled on ice, a probe-tip sonicator (Sonics Vibra Cell; Sonics & Materials) was used to generate small unilamellar vesicles (SUVs) from the lipids. Debris was removed by centrifugation at 20,000 × g at 4 °C for 3 h, and the supernatant containing the SUVs was transferred to a fresh tube. All lipid vesicles were stored at 4 °C until further use.

For preparing supported lipid bilayers, glass coverslips were first cleaned by sonication in a 1:1 mixture of isopropanol and water for 15–30 min. After extensive rinsing with water, coverslips were further cleaned either by incubating in fresh Piranha solution [3:1 (vol/vol) mixture of H_2SO_4: 30% H_2O_2] for 5 min or in 50% H_2SO_4 overnight or by UV treatment in an enclosed UV Ozone generator (UV/Ozone ProCleaner Plus; Bioforce Nanosciences) for 30 min. Glass coverslips were then rinsed extensively and dried under an N_2 stream. Bilayers were self-assembled on the glass coverslips by incubating a 1:1 mixture of lipid vesicles and 2 × Tris buffered saline (TBS; Sigma-Aldrich) for 5 min, and the bilayer-containing coverslips were each assembled into Attofluor Cell Chambers (Life Technologies) for further experiments. Chromium grid-patterned substrates were prepared as described previously (73).

Functionalization of Supported Lipid Bilayers with E-cad-ECD. Supported lipid bilayers assembled in Attofluor Cell Chambers were rinsed with 15 mL TBS and blocked with 0.01% BSA in TBS for 30 min. In some experiments, bilayers were incubated with 150 nM $NiCl_2$ for 5 min before blocking to saturate the NTA-DOGS lipids in the bilayers with complexed Ni^{2+}. Bilayers were rinsed with 15 mL of TBS containing 1 mM $CaCl_2$ (TBS + Ca^{2+}). Protein stock (2 mg/mL) was diluted with TBS + Ca^{2+} and added to the bilayer at a final concentration of 30 nM. The protein was incubated at room temperature for 90 min and then rinsed with 15 mL TBS + Ca^{2+}. After an additional 30-min incubation, the bilayer was rinsed with 15 mL TBS + Ca^{2+} to remove unbound protein molecules from the bilayer. For live cell experiments, the solution was exchanged with an imaging buffer (50 mM Hepes, 150 mM NaCl, 5 mM KCl, 1 mM $MgCl_2$, 11.1 mM D-glucose, 2 mM $CaCl_2$, pH 7.4).

Imaging FRAP. For FRAP analysis, the field diaphragm of the Eclipse Ti inverted microscope (Nikon) was closed partway to allow only a 15- to 30-μm-diameter field of view on the bilayer with a 100× oil immersion objective. The excitation light was turned on continuously at a high intensity to bleach the fluorophore for 1–2 min, or until noticing a decrease in emitted signal. Then, the excitation light intensity was returned to its previous value, and, immediately, the field diaphragm was opened completely. Time-lapse imaging was started with an image recorded at appropriate intervals to monitor recovery of fluorescence at the photobleached region.

FCS. A 5-ps pulsed super continuum laser (SuperK Extreme; NKT Photonics) was used to illuminate a diffraction-limited spot on a bilayer sample through a 100× oil objective on an Eclipse Ti inverted microscope. The laser excitation wavelength was selected with an acoustooptic tunable filter set to 568 nm (∼5-nm bandwidth). Photons were detected by single-photon avalanche photodiodes (Micro Photon Devices) and recorded with the PicoHarp 300 photon-counting module (PicoQuant) with a time resolution of 32 ps. Photon arrivals were collated into 10-μs time bins and analyzed for autocorrelation using custom built codes (73, 74) in Matlab (MathWorks). For Z-scan FCS analysis of bilayer samples, the stage was moved 500 nm above and 500 nm below the bilayer in either 50-nm or 100-nm steps. FCS data were analyzed at each *z* position and fit to an autocorrelation function for normal 2D diffusion in a 2D Gaussian illumination spot,

$$G(\tau) = \frac{1}{\langle N \rangle}\left(\frac{1}{1+\tau/\tau_D}\right),$$

where $\langle N \rangle$ represents average number of particles and τ_D represents the mean residence time of those particles in the illumination spot. Values of $\langle N \rangle$ and τ_D determined at each z position were plotted against a floated square of z displacement and y intercepts of the best linear fits provided the $\langle N \rangle$ and τ_D values at the minimum beam waist. Beam waist was calibrated by performing Z-scan FCS analyses on DOPC bilayers containing a range of known molecular densities of TexasRed-DHPE and was found to be diffraction-limited ($w = 0.21$ μm). The diffusion coefficient was calculated from dwell time using $D = w^2/4\tau_D$.

For PCH analysis, the recorded photon arrivals were first binned in 200-μs sampling time intervals to obtain photon counts. The histogram of the photon counts was then normalized to yield a photon probability distribution. The histograms were later analyzed using the Globals software package developed at the Laboratory for Fluorescence Dynamics at the University of Illinois at Urbana–Champaign. The excitation was assumed to be 2D Gaussian, and both single-species and two-species models were used for the analysis.

Cell Culture and Preparation of Cells for Live Cell Experiments. MKN-28 cells were grown in Roswell Park Memorial Institute (RPMI) 1680 supplemented with 10% fetal bovine serum (FBS) and 1% penicillin/streptomycin, at 37 °C and in an atmosphere of 5% CO_2. A-431D cells expressing wild-type, *cis*-mutant, and intracellular domain-deleted E-cadherin described previously (65) were grown in DMEM with 10% FBS and 1% penicillin/streptomycin, at 37 °C and in an atmosphere of 5% CO_2. MCF-10A cells were grown in DMEM-F12 with 5% horse serum (Life Technologies), 20 ng/mL EGF (Life Technologies), 10 μg/mL bovine insulin (Sigma-Aldrich), and 500 ng/mL hydrocortisone (Sigma-Aldrich). For live cell experiments, cells were washed with either Dulbecco's PBS or PBS and detached by incubating with Cell Stripper (Life Technologies), an enzyme-free cell dissociation buffer, for 10–20 min at 37 °C. Detached cells were gently pipetted to produce single cells. The cell suspension was centrifuged and the cells were resuspended in the imaging buffer.

In Vitro Binding of Fluorescently Labeled E-cad-ECD to Glass Surface Coated with Human E-cad-ECD. Coverslips were cleaned as described previously and coated with 40 μL of 250 μg/mL solution of human E-cad-ECD (Sino Biological Inc.) prepared in TBS + 1 mM $CaCl_2$ by incubation at room temperature for 2 h. Coverslips were assembled into Attofluor Cell Chambers (Life Technologies) and washed with 15 mL of either TBS alone (for monitoring binding in the absence of Ca^{2+}) or TBS + 1 mM $CaCl_2$ (for monitoring binding in the presence of Ca^{2+}) buffer to remove unbound protein. For monitoring initial binding, fluorescently labeled E-cad-ECD was added to the glass surfaces and imaged in the total internal reflection fluorescence (TIRF) mode. For determining total binding, the glass surfaces were washed with 15 mL of buffer (either TBS or TBS + 1 mM $CaCl_2$) and imaged in the epifluorescence mode. Molecular density was determined by quantitative fluorescence imaging using a DOPC bilayer containing 0.005% TexasRed-DHPE as a standard.

Cell Adhesion on Glass Surfaces. Dry, hydrophilic, UV-treated coverslips were each incubated with 1.5 μg protein in 40 μL TBS + 1 mM $CaCl_2$ for 2 h. The proteins used were BSA as control and fluorescently labeled Ecad-ECD. After the coverslips were assembled into Attofluor Cell Chambers (Life Technologies), they were rinsed with buffer and filled with RPMI media with 10% FBS and 1% penicillin/streptomycin. MKN-28 cells were dissociated from culture dishes with Cell Stripper, and 1.2×10^6 cells were seeded into each cell chamber. Following a 4-h incubation, the samples were rinsed thoroughly with 10 mL TBS + 1 mM $CaCl_2$ each, and five images were taken of each sample with transmitted light using an inverted microscope and a 40× air objective. The cells were counted in the central 500 μm × 500 μm region of each image for quantification.

Immunostaining of Fixed Cells and Western Blot Analysis. Following 1–3 h of incubation on the bilayer with imaging buffer, samples were rinsed with Dulbecco's PBS. The cells were fixed with 4% paraformaldehyde for 12 min, and the cell membrane was permeabilized with 0.1% Triton-X for 5 min. After blocking in 1% BSA for 30 min, cells were immunostained with primary antibodies and fluorescent secondary antibodies. The antibody against the cytoplasmic domain of E-cadherin was purchased from BD Biosciences; the antibody against its extracellular domain was purchased from Santa Cruz Biotechnology. The α-catenin antibody was purchased from Sigma-Aldrich, as was fluorescently labeled phalloidin. Fluorescent secondary antibodies were purchased from Life Technologies. Western blot analysis of cell lysates for E-cadherin was performed with an antibody raised against the cytoplasmic domain of E-cadherin (BD Biosciences), for β-catenin with a rabbit monoclonal antibody raised against β-catenin (Abcam), and for α-catenin with a rabbit polyclonal antibody raised against α-catenin (Sigma-Aldrich). Densitometry analysis of chemiluminescence for quantification of E-cadherin level was performed using ImageJ.

Assay for Junction Formation on Bilayers and Quantification. Single-cell suspensions prepared as described above were added to various bilayers and imaged by epifluorescence or confocal microscopy. For the purpose of quantification, cells were allowed to interact with bilayers for 1 h, and bilayers were washed with 15 mL of chilled DPBS to remove unbound cells. Cells were fixed with paraformaldehyde before imaging and quantification. To test the effect of serum on the ability of cells to form junctions, cells were seeded on bilayers in the presence of imaging buffer containing 10% FBS. To test the effect of membrane tension on junction formation by cells, 30% of the imaging buffer in the cell culture chamber was exchanged with water followed by addition of cells. Cells were pretreated for 30 min with 100 μM of ML 141 to inhibit Cdc42, 1 nM of Calyculin A to inhibit protein phosphatase, 50 μM blebbistatin for inhibiting myosin II, and a combination of 5 mM 2'-deoxy glucose and 1 μM antimycin A for depleting ATP levels in cells. All drug treatments were continued in the course of the experiment. Cells that showed any enrichment of E-cad-ECD on the bilayer were counted as positive for junction formation.

Generation of E-cadherin and α-Catenin Actin Binding Domain Fusion Protein. For the generation of E-cadherin and α-catenin fusion protein, a 213-bp fragment (β-catenin binding site) from the C terminus of mouse E-cadherin was deleted from pRZB26 (pSpeckle-E-cadherin-mCherry) and replaced with a 2.5-kb Not1 fragment from pUC-α-catenin-GFP. This Not1 fragment from pUC-α-catenin-GFP lacks the 897 base pairs from the N terminus of α-catenin, in addition to GFP ORF being inserted between the adhesion modulation domain and F-actin binding domain of α-catenin.

Imaging. An Eclipse Ti inverted microscope (Nikon) with a CSU-X1 confocal spinning disk unit (Yokogawa) and Evolve electron multiplying charge-coupled device (EMCCD) camera (Photometrics) was used for fixed and live cell images. For some cell images, an Eclipse Ti inverted microscope (Nikon) with the same camera was used for epifluoresence, RICM, and TIRF imaging. Images were collected in Metamorph (Molecular Devices) and

analyzed with ImageJ (National Institutes of Health). TIRF microscopy was performed with a 100× TIRF objective with a numerical aperture of 1.49 (Nikon) and an iChrome MLE-L multilaser engine as a laser source (Toptica Photonics).

SI Results

Labeled E-cad-ECD Shows Binding. The activity of labeled E-cad-ECD was tested in the following ways. First, we observed direct binding of the fluorescently labeled E-cad-ECD to nonlabeled E-cad-ECD coated on a glass surface. TIRF microscopy revealed the initial binding of E-cad-ECD to E-cad-ECD-coated glass only in the presence of Ca^{2+} (Fig. S1*C*). Quantitative epifluorescence microscopy showed the total binding after 1-h incubation (Fig. S1*D*). Second, a higher number of cells adhered to the E-cad-ECD-coated glass surface than the control surface in a typical cell adhesion assay (Fig. S1 *E* and *F*). These observations confirmed that the fluorescently labeled E-cad-ECD was active, and could potentially allow formation of a hybrid junction between live cells and artificial bilayers.

Cellular E-cadherin Is Preserved While Preparing Cells for Assay. To preserve cellular E-cadherin for live cell experiments, cells cultured at low densities were detached with enzyme-free dissociation buffer and immediately resuspended as single cells in an imaging buffer that included Ca^{2+} and glucose (Fig. S1 *G* and *H*).

Estimation of Force Generated by Retracting Filopodia. We estimated the force generated by retracting filopodia on E-cad-ECD molecules on fluid bilayers using the Einstein–Smoluchowski relation: Using $D = \mu k_B T$ and $V = \mu F$, we get

$$F = \frac{V}{\mu} = \frac{V k_B T}{D}.$$

Filopodia retraction velocities on a fluid bilayer were determined to be 180 ± 160 nm/s by tracking RICM images. By substituting values for $V = 180$ nm/s, $k_BT = 4.28$ pN·nm at $T = 310$ K, and $D = 1.6$ μm^2/s obtained from FCS measurements, we find an average force of 0.5 fN that would be experienced by each E-cad-ECD molecule on a fluid bilayer. This magnitude of force is much lower than the 30 pN of critical force reported for the X-dimer catch bond (61).

Characterization of Junctions Formed on Fluid Bilayers. RICM (75) imaging of cells that formed junctions on bilayers revealed a reduction of reflected light intensity at regions of E-cad-ECD enrichment on the bilayer (Fig. S2*A*), confirming a close association of the cell to the E-cad-ECD functionalized membrane surface. FCS analysis of E-cad-ECD positions in the supported membrane outside of adhesive regions exhibited free movement, comparable to the behavior of the protein in supported membranes in the absence of cells (Fig. S2*B*). However, FCS measurements within points of adhesion in the hybrid live cell-supported bilayer junction exhibited substantial reductions in mobility as evidenced from the large shift in their autocorrelation curves (Fig. S2*B*). This is similar to the observation of low-mobility E-cadherin upon formation of junctions between two cells (15).

Low Frequency of E-cadherin Junctions on Fluid Bilayers. Very few cells seeded on fluid E-cad-ECD bilayers formed junctions. Instead, most cells showed a weak nonspecific interaction with the bilayer. This nonspecific interaction reduced the fluorescence intensity on the bilayer in certain cases, suggesting an exclusion of the protein at the cell–bilayer interface. Because this also occurred in the absence of Ca^{2+}, we presume that the cell interacted with the exposed Ni-NTA groups on the bilayer.

To rule out the possibility that the low frequency of junction formation on fluid bilayer is due to low E-cadherin density, we either functionalized bilayers with higher concentrations of E-cad-ECD (Fig. S3*A*) or overexpressed GFP-tagged E-cadherin in the cells (Fig. S3*C*). However, these changes did not result in any noticeable increase in the frequency of junction formation (Fig. S3 *B*, *D*, and *E*). Other cell lines such as S180-E-cad-GFP, MDCK-E-cad-GFP, or A-431 that are frequently used for studying E-cadherin-mediated cell–cell junction also failed to efficiently form junctions on fluid bilayers (Fig. S3 *D* and *E*), ruling out any cell type-specific effect.

Movement of vascular endothelial (VE)-cadherin clusters on the lateral membrane of A-431 cells has been shown to be dependent on the presence of serum (76). Also, membrane tension induced by hypotonic swelling of cells was reported to result in an increased accumulation of VE-cadherin at junctions formed on a glass surface (77). However, incubation of cells in the presence of serum or in hypotonic solution did not result in any significant increase in the frequency of junction formation (Fig. S3 *F*–*I*).

We further tested if adhesion between cells mediated by noncadherin adhesion proteins would influence the formation of cadherin junction-like structures. To this end, we seeded MCF-10A cells, a breast epithelial cell line that expresses E-cadherin, EphA2, and integrins, on fluid bilayers functionalized with either EphrinA1 or RGD peptide in addition to E-cad-ECD (Fig. S3 *J* and *K*). With these cells, robust contacts (95% of cells) were observed between the cells and a supported membrane coated with EphrinA1; similarly, the expressed integrin mediates robust attachment to an RGD-peptide-coated membrane (93% cells) (Fig. S3 *L* and *M*). Nevertheless, the adhesion between these cells and the supported bilayers did not result in increased clustering of E-cadherin (Fig. S3 *L* and *M*).

Junction Formation on Bilayers with Different Compositions. The diffusive properties of E-cad-ECD bilayers were varied by altering their lipid compositions. Bilayers prepared using DPPC doped with 1 mole % NBD-PC lipid molecules for E-cad-ECD functionalization showed very slow micrometer-scale diffusion of E-cad-ECD (referred to as a partially fluid bilayer) (Fig. S4). NBD-PC contains the bulky fluorescent 7-nitro-2–1,3-benzoxadiazol-4-yl-amino group as a part of one of its acyl chains, thus interfering with the ordering of the DPPC acyl chains in the bilayer (51). Fluorescence intensity analysis showed a similar density of E-cad-ECD on these bilayers compared with fluid bilayers (relative intensity of 1.6 ± 0.6 compared with fluid bilayers). In contrast to fluid bilayers, intensity fluctuations of E-cad-ECD on these surfaces could not be measured due to the faster onset of photobleaching. Gel-phase bilayers prepared using DPPC without NBD-PC did not allow reorganization of E-cad-ECD, although individual E-cad-ECD could interact with cellular E-cadherin as evidenced from greater spreading of the cells on the bilayers.

Bilayers containing 4 mole % Ni-NTA against a combination of DPPC and DOPC showed decreasing mobility of E-cad-ECD with increasing DPPC concentration as judged from FRAP assays (Fig. S5 *A*–*E*). However, cells failed to efficiently form junctions on any of these bilayers.

Increased Frequency of Junction Formation on DPPC Bilayers at 42 °C. Although cells failed to efficiently form junctions on DPPC bilayers at 37 °C, increasing the experimental temperature from 37 °C to 42 °C allowed efficient E-cadherin junction formation on these bilayers (Fig. S6*A*). Although 42 °C is higher than the melting temperature of pure DPPC vesicles (41 °C), it may not result in a dramatic increase in the mobility of E-cad-ECD molecules bound to Ni-NTA-DOGS in the DPPC bilayer because the phase transition occurs via formation of disordered domains, and the melting curves of bilayers are often more spread out than that of vesicles (53).

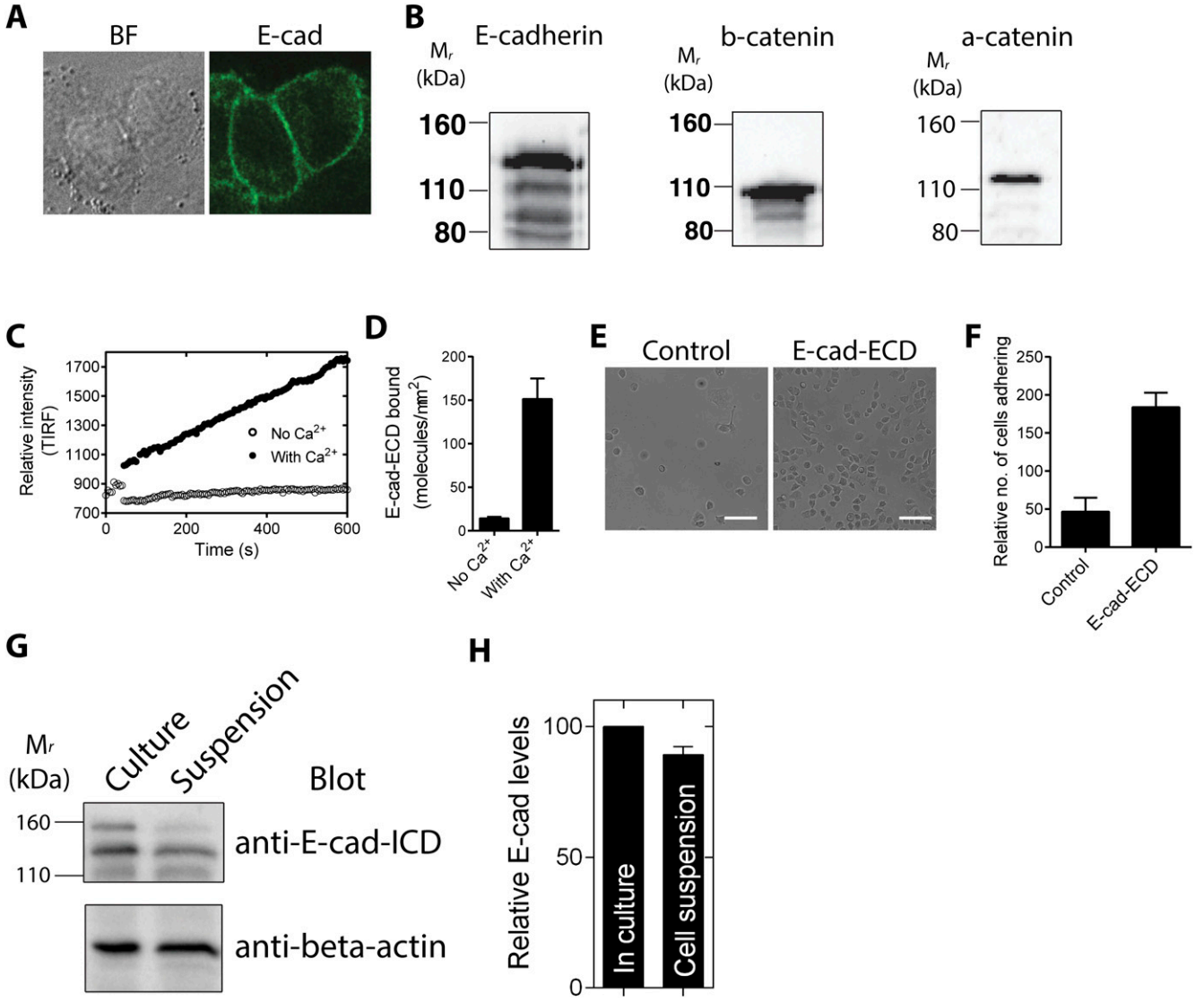

Fig. S1. (*A*) Bright field and confocal image of MKN28 cells forming junctions in culture and stained with an antibody raised against the intracellular domain of E-cadherin. (*B*) Western blot analysis of lysates prepared from a confluent monolayer of MKN28 cells probed for E-cadherin, β-catenin, and α-catenin. (*C*) Initial binding of fluorescently labeled E-cad-ECD to glass-adsorbed, nonlabeled E-cad-ECD in the presence and absence of Ca^{2+}, monitored by TIRF microscopy. (*D*) Binding of fluorescently labeled E-cad-ECD to nonlabeled E-cad-ECD adsorbed on a glass surface in the presence and absence of Ca^{2+}. (*E* and *F*) Bright field image (*E*) and quantification (*F*) of MKN28 cells adhering to either negative control (BSA) or E-cad-ECD coated glass surface. (Scale bar, 100 μm.) (*G*) (*Top*) Western blot analysis of lysates prepared from MKN28 cells in either culture or suspension, probed with an antibody against the intracellular domain of E-cadherin. (*Bottom*) The same blot probed with anti-beta actin antibody. (*H*) Relative level of E-cadherin in lysates prepared from MKN28 cells in either culture or suspension, quantified from chemiluminescence signal using ImageJ.

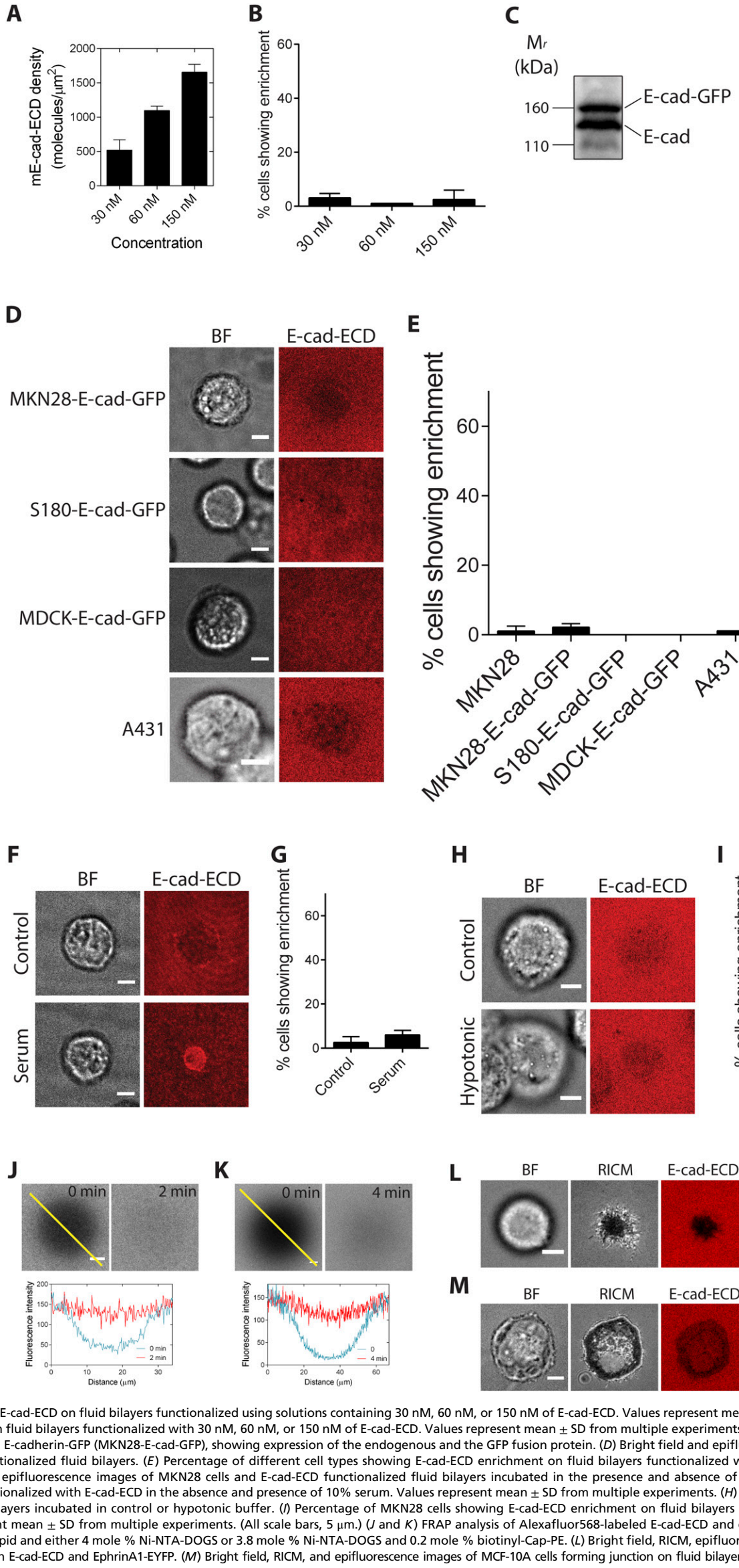

Fig. S2. (*A*) Molecular density of E-cad-ECD on fluid bilayers functionalized using solutions containing 30 nM, 60 nM, or 150 nM of E-cad-ECD. Values represent mean ± SD from an experiment. (*B*) Percentage of MKN28 cells showing E-cad-ECD enrichment on fluid bilayers functionalized with 30 nM, 60 nM, or 150 nM of E-cad-ECD. Values represent mean ± SD from multiple experiments. (*C*) Western blot analysis of lysates prepared from MKN28 and MKN28 cells stably expressing E-cadherin-GFP (MKN28-E-cad-GFP), showing expression of the endogenous and the GFP fusion protein. (*D*) Bright field and epifluorescence images of S180-Ecad-GFP, MDCK-E-cad-GFP, and MKN28 cells with E-cad-ECD functionalized fluid bilayers. (*E*) Percentage of different cell types showing E-cad-ECD enrichment on fluid bilayers functionalized with E-cad-ECD. Values represent mean ± SD from multiple experiments. (*F*) Bright field and epifluorescence images of MKN28 cells and E-cad-ECD functionalized fluid bilayers incubated in the presence and absence of serum. (*G*) Percentage of MKN28 cells showing E-cad-ECD enrichment on fluid bilayers functionalized with E-cad-ECD in the absence and presence of 10% serum. Values represent mean ± SD from multiple experiments. (*H*) Bright field and epifluorescence images of MKN28 cells and E-cad-ECD functionalized fluid bilayers incubated in control or hypotonic buffer. (*I*) Percentage of MKN28 cells showing E-cad-ECD enrichment on fluid bilayers functionalized with E-cad-ECD and incubated in control or hypotonic buffer. Values represent mean ± SD from multiple experiments. (All scale bars, 5 μm.) (*J* and *K*) FRAP analysis of Alexafluor568-labeled E-cad-ECD and either EphrinA1-EYFP (*J*) or RGD (*K*) functionalized bilayers prepared with DOPC as the base lipid and either 4 mole % Ni-NTA-DOGS or 3.8 mole % Ni-NTA-DOGS and 0.2 mole % biotinyl-Cap-PE. (*L*) Bright field, RICM, epifluorescence, and TIRF images of MCF-10A cells forming junction on fluid bilayers functionalized with E-cad-ECD and EphrinA1-EYFP. (*M*) Bright field, RICM, and epifluorescence images of MCF-10A cells forming junction on fluid bilayers functionalized with E-cad-ECD and RGD. (Scale bar, 5 μm.)

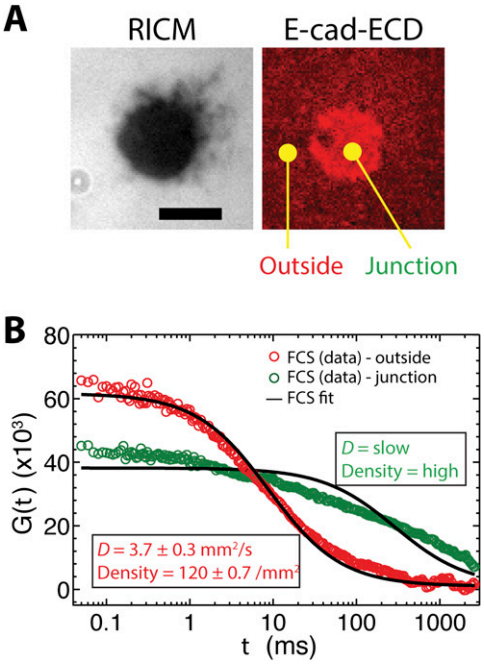

Fig. S3. Junction formation results in a reduction in diffusion of E-cad-ECD. (*A*) RICM and epifluorescence image of a hybrid junction formed between a live cell and E-cad-ECD functionalized fluid bilayer. (*B*) FCS curve fit to a standard 2D, single-component diffusion model of spots outside and inside the hybrid junction indicated in *A*. Note that the intensity fluctuation of E-cad-ECD inside the junction could not be fit to a simple, single-component model indicating the presence of clusters that do not show random Brownian diffusion. (Scale bar, 5 μm.)

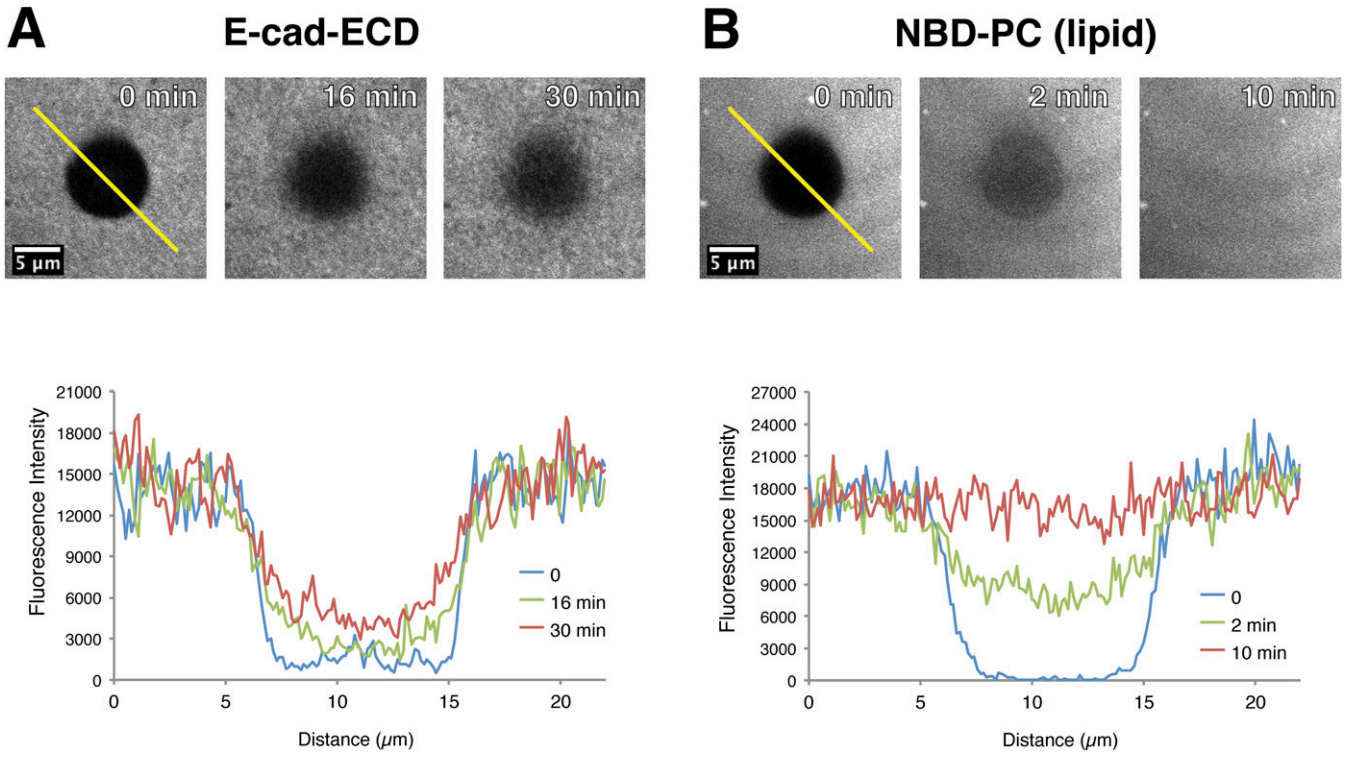

Fig. S4. FRAP analysis of partially fluid E-cad-ECD functionalized bilayer. (*Top*) Recovery of fluorescence intensity of labeled E-cad-ECD (*A*) and NBD-PC (*B*) and (*Bottom*) corresponding line scans of the images. Diffusion coefficient of NBD-PC was estimated to be 0.04 $\mu m^2/s$. Diffusion coefficient of E-cad-ECD could not be estimated due very low recovery of fluorescence intensity.

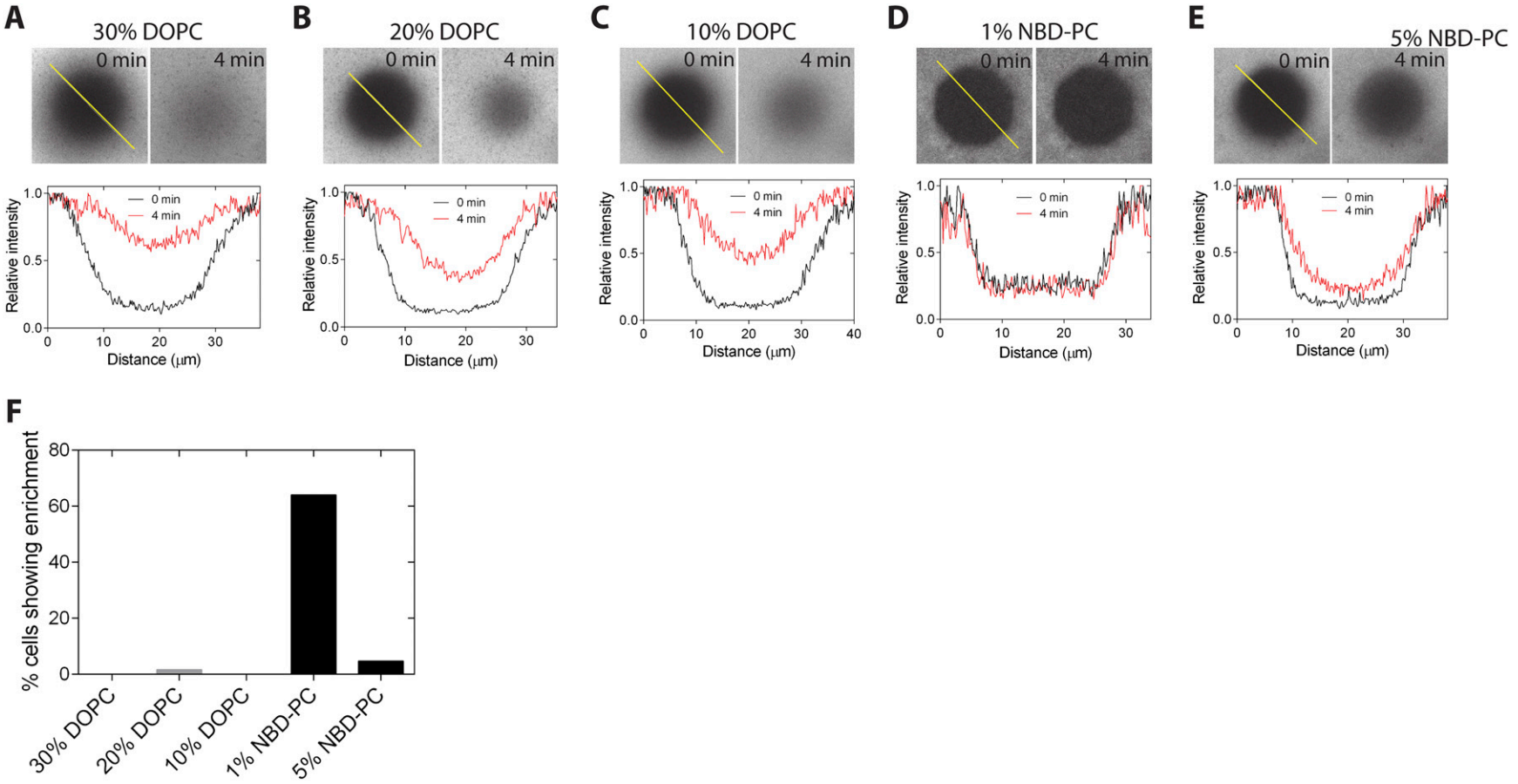

Fig. S5. FRAP analysis of Alexafluor568-labeled E-cad-ECD functionalized bilayers prepared with DPPC as the base lipid and 30 mole % DOPC (*A*), 20 mole % DOPC (*B*), 10 mole % DOPC (*C*), 1 mole % NBD-PC (*D*), and 5 mole % NBD-PC (*E*). All bilayers contained 4 mole % Ni-NTA-DOGS lipid for anchoring the protein. (*Top*) The photobleached spots at 0-min and 4-min time periods, and (*Bottom*) line scans of the images at the indicated position (yellow line in *Top*). (*F*) MKN28 cells were seeded on bilayers with different lipid compositions, and then the cells showing enrichment of E-cadherin were counted to determine their percentage.

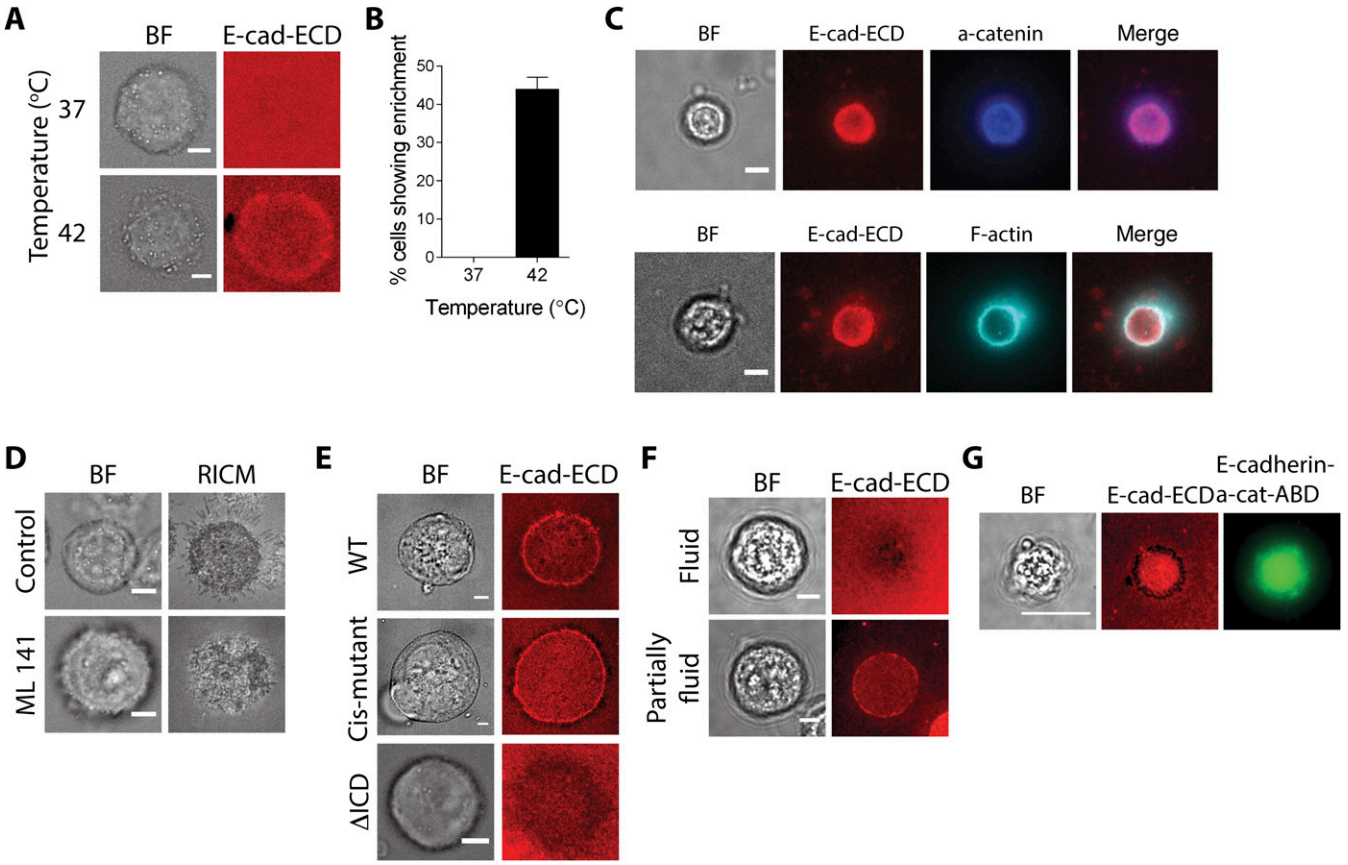

Fig. S6. (*A*) Bright field and epifluorescence images of MKN28 cells seeded on DPPC bilayers incubated at the indicated temperatures. (*B*) Percentage of MKN28 cells showing E-cad-ECD enrichment on DPPC bilayers incubated at the indicated temperatures. Values represent mean ± SD. (Scale bar, 5 μm.) (*C*) MKN-28 cells forming junctions on fluid bilayers were either immunostained with an antibody against α-catenin or stained with phalloidin. Cellular α-catenin colocalize with E-cad-ECD molecules on the bilayer whereas F-actin is remodeled to form a ring around the hybrid junction. (Scale bar, 5 μm.) (*D*) Bright field and RICM images of MKN28 cells, on partially fluid bilayers with E-cad-ECD, with and without ML 141 treatment. (Scale bar, 5 μm.) (*E*) Bright field images of A-431D cells expressing wild-type, *cis*-mutant, or intracellular domain-deleted E-cadherin, seeded on partially fluid bilayers functionalized with wild-type, *cis*-mutant, or wild-type E-cad-ECD, respectively, and epifluorescence images of fluorescently labeled protein showing formation of junction. (Scale bar, 5 μm.) (*F*) Bright field images of MKN28 cells expressing E-cadherin fused to the actin-binding domain of α-catenin, seeded on either a fluid or partially fluid bilayer, and epifluorescence images of E-cad-ECD showing formation of junction. (*G*) Bright field and epifluorescence images of an MKN28 cell with the E-cadherin-α-catenin actin-binding domain fusion protein forming a junction with E-cad-ECD on a partially fluid bilayer. (Scale bar, 10 μm.)

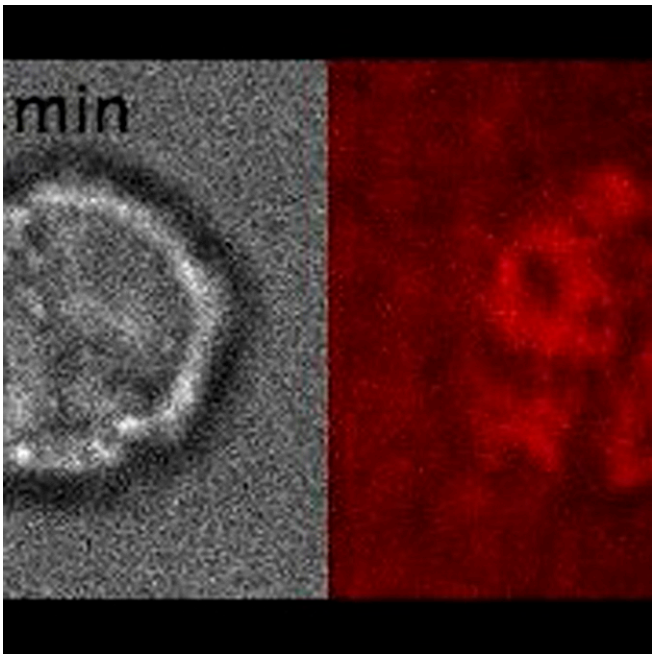

Movie S1. Time lapse bright field and epifluorescence movie of a cell that is forming junction on an E-cad-ECD functionalized fluid DOPC bilayer.

Movie S1

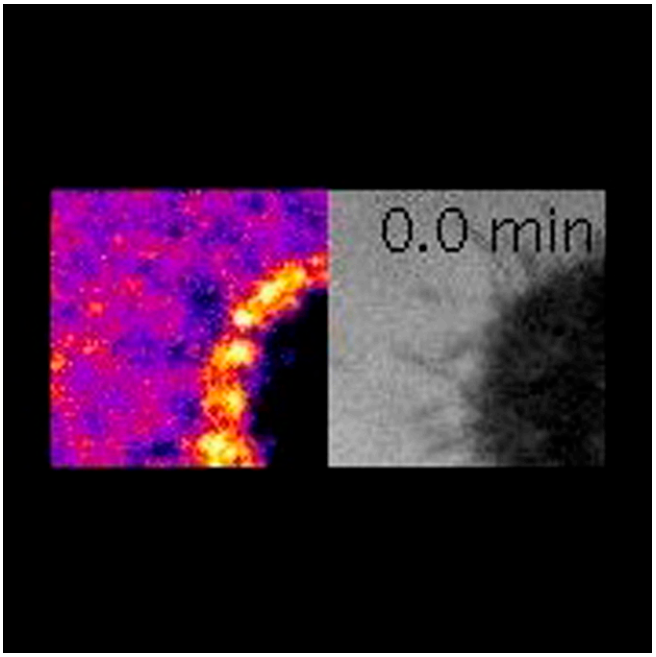

Movie S2. Time lapse RICM and epifluorescence movie of a retracting filopodia of a cell resulting in the clustering of E-cad-ECD on an E-cad-ECD functionalized partially fluid DPPC+NBD-PC bilayer.

Movie S2